APL Materials

Enhanced electric polarization and breakdown strength in the all-organic sandwich-structured poly(vinylidene fluoride)-based dielectric film for high energy density capacitor

Cite as: APL Mater. **5**, 076109 (2017); https://doi.org/10.1063/1.4995653
Submitted: 05 May 2017 • Accepted: 12 July 2017 • Published Online: 25 July 2017

Yue Zhang, Qingguo Chi, Lizhu Liu, et al.

Enhanced electric polarization and breakdown strength in the all-organic sandwich-structured poly(vinylidene fluoride)-based dielectric film for high energy density capacitor

Yue Zhang,[1,2] Qingguo Chi,[1,3,4,a] Lizhu Liu,[1,2] Changhai Zhang,[1,2] Chen Chen,[1,3] Xuan Wang,[1,3] and Qingquan Lei[1]

[1]*Key Laboratory of Engineering Dielectrics and Its Application, Ministry of Education, Harbin University of Science and Technology, Harbin 150080, People's Republic of China*
[2]*School of Materials Science and Engineering, Harbin University of Science and Technology, Harbin 150080, People's Republic of China*
[3]*School of Electrical and Electronic Engineering, Harbin University of Science and Technology, Harbin 150080, People's Republic of China*
[4]*State Key Laboratory of Electronic Thin Films and Integrated Devices, University of Electronic Science and Technology of China, Chengdu 610054, People's Republic of China*

(Received 5 May 2017; accepted 12 July 2017; published online 25 July 2017)

It is essential to develop the dielectric energy storage capacitor for the modern electrical and electronic equipment. Here, the all-organic sandwich-structured composite with superior breakdown strength and delayed saturation polarization is presented. Furthermore, the energy storage characteristics of the composite are enhanced by the poly(vinylidene fluoride-trifluoroethylene-chlorofluoroethylene) fiber and the redistribution of local electric field. The dielectric permittivity of composite increases to ~16, and the discharged energy density is high to ~8.7 J/cm^3 at 360 kV/mm, and the breakdown strength is up to ~408 kV/mm. The excellent performance of the composite broadens the application in the field of power electronics industry.
[http://dx.doi.org/10.1063/1.4995653]

It is an urgent requirement to develop a high performance energy storage capacitor for the advanced electronics and electrical power system. The dielectric materials have drawn the worldwide attention of researchers for their widely applications,[1–4] such as dielectric-based capacitors[2] and hybrid electric vehicles.[3] Especially, the polymer dielectric materials possess the advantages of lightweight, low-cost and multi-functionality in the power electronic system. At present, the state-of-the-art dielectric capacitor in commercial application is the biaxially oriented polypropylene (BOPP). The highest energy storage density of BOPP is about 2 J/cm^3 and the permittivity is about 2.2,[4] which cannot meet the growing demand for the efficient and reliable power electronics.[5] Therefore, it is imperative to develop a novel capacitor material which possesses significantly increased dielectric permittivity and energy density. The formula,

$$U_e = \int_{D_{max}}^{0} E \cdot dD, \tag{1}$$

is used to express the energy storage density of nonlinear dielectrics, where E represents the electric field and D means the electric displacement, which is related to the electric polarization P and the relative permittivity ε_r by $D = P + \varepsilon_r\varepsilon_0 E$.[6] Therefore, it is very crucial to combine the high dielectric permittivity and high breakdown strength to obtain the composite with a high energy storage density.

[a]Electronic mail: qgchi@hotmail.com

Moreover, ceramic fillers with high dielectric permittivity are preferred to combine with a high electric field polymer matrix to improve the electric displacement and enhance the energy density of composite.[7–11] Generally speaking, the introduction of the second phase particles[5,7–13] will lead to the following problems. First, the significant dielectric difference between the fillers and the matrix, resulting in the concentration of the local electric field at the interface, reduces the breakdown field strength.[14] Second, the relative specific surface area of the nano-fillers is larger, which gives rise to poor dispersion and particles agglomeration reducing the performance.[8,13] Finally, the preparation process of composite becomes complicated by the modification on the surface of the particles.[3] In short, they are not conducive to improving the energy density.[15] Therefore, the all-polymer dielectric material was prepared by a simple and quick method in this paper. The bright points of the all-polymer dielectric composite are mainly about good compatibility, excellent flexibility, and great breakdown strength.[12,16–18] Meanwhile, to block the extension of the inner electrical treeing, the sandwich-structured composite was prepared.[19–22] Herein, a novel all-organic sandwich-structured composite was fabricated. The central layer of poly(vinylidene fluoride-trifluoroethylene-chlorofluoroethylene) (P(VDF-TrFE-CFE)) fiber (PTCF) film, which owns a higher relative permittivity $\varepsilon_r \sim 56$,[23] was produced by the electrospinning technique. The outer layer of poly(vinylidene fluoride) (PVDF) film (P in short) was gained by a simple and quick solution-casting method.

The P(VDF-TrFE-CFE) fibers with high aspect ratios were prepared by an electrospinning technique.[24] And the films were fabricated by the simple and quick solution-casting method (more details are given in the supplementary material). Then the sandwich-structured films were fabricated by a hot-pressing process shown in Fig. S1 of the supplementary material. Finally, the multilayer films were heated at 200 °C for 7 min and then quenched in ice water immediately. The X-ray diffraction (XRD) patterns of composites are shown in Figs. 1(a) and 1(b).

The non-polar α phase and polar β phase were formed in the sandwich-structured composites with PTC and PTCF layers without the quenching process in the XRD patterns. And the diffraction peaks of α phase were at 17.9° and 20.2° which could be assigned to α(100) and α(021); the peaks of β phase were at 20.7° and 20.8° which could be assigned to β(200) and β(110).[5,24] The non-polar γ phase is preferred to be formed, which is induced by the quenching process in the PVDF

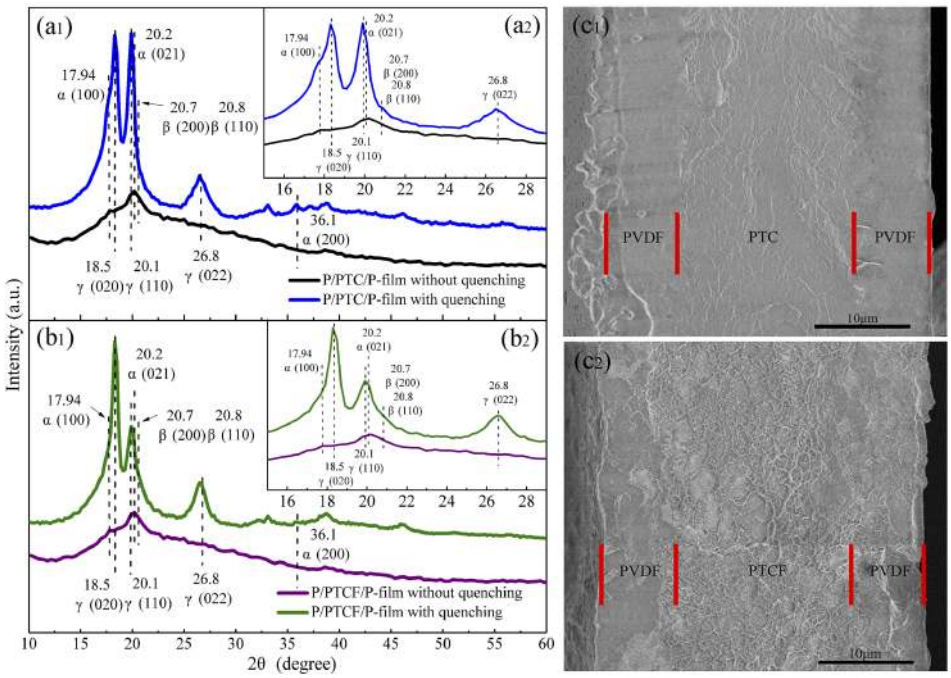

FIG. 1. The X-ray diffraction patterns (a) and (b); the SEM of cross-sectional morphology (c) for the sandwich-structured composite.

and the P(VDF-TrFE-CFE),[5,25] and the diffraction peaks at 18.5°, 20.1°, and 26.8° could be ascribed to γ(020), γ(110), and γ(022), respectively.[24] As shown in Fig. S2 of the supplementary material, it can be found that the non-polar γ phase in the P/PTCF/P composite with quenching is more obvious than that in the P/PTC/P composite with quenching, which may be caused by the central P(VDF-TrFE-CFE) fibers under the quenching process. It is desirable to achieve the γ phase, which can reduce ferroelectric loss, improve breakdown strength, and weaken early polarization saturation.[25] Meanwhile, the non-polar γ phase holds a smaller polarizability than the polar β phase that can suppress the remnant displacement (D_r) of composites.[23,24,26]

According to the SEM results, the thickness ratio between the outer pure P layer and central PTC layer or PTCF layer was about 9:16:9. The SEM of cross-sectional morphology for the sandwich-structured composite with the central layer of the PTC film, in Fig. 1(c1), reveals that the central PTC film is well compatible with the outer layers, which are the compact layers and possess fewer defects. And the cross-sectional morphology of the sandwich-structured film with PTCF, in Fig. 1(c2), indicates that the outer P layers cast from solution are dense and a little pores or voids in the film. And the central layer of PTCF, which was well-preserved, is compatible with the outer P layers. These sandwich structures are advantageous for improving the dielectric performances and energy storage properties of the films.

The frequency-dependent dielectric permittivity, dielectric loss, and conductivity of sandwich-structured composites are presented in Fig. 2(a). With the frequency increasing, the dielectric permittivity of all films tends to gradually decrease, while the conductivity of every film increases, because the motion of amorphous phase dipolar in the films could not follow the switching of the

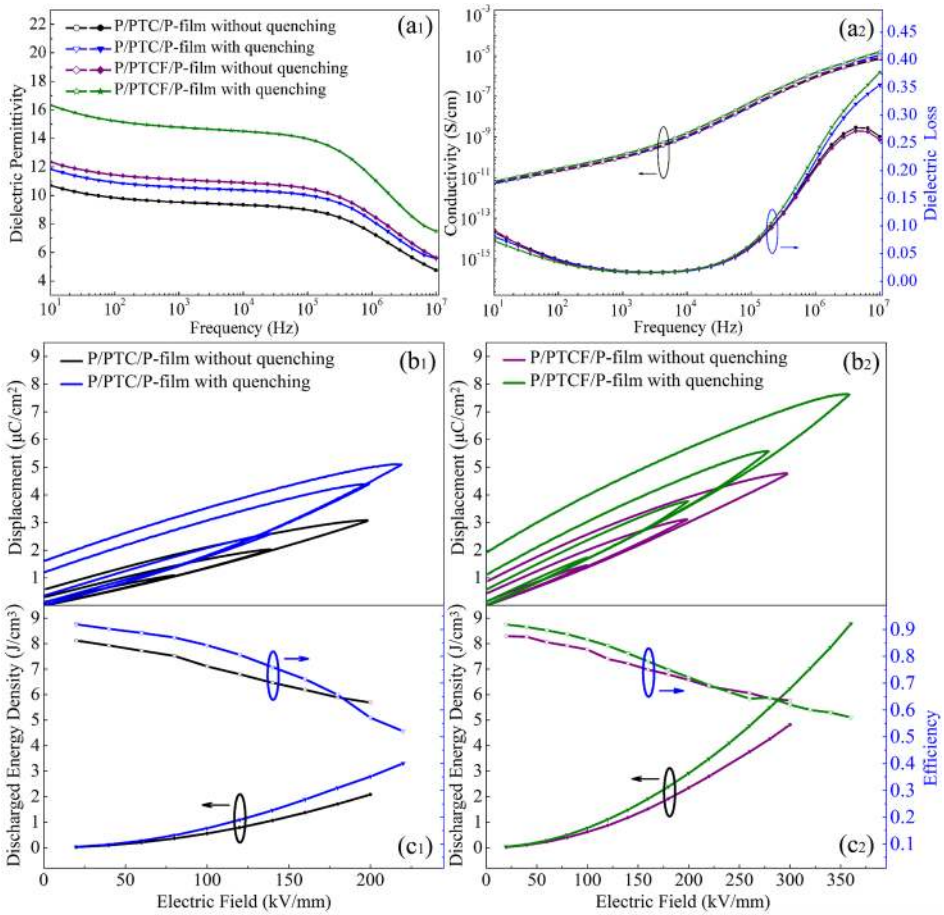

FIG. 2. The dielectric properties (a); displacement-electric field (D-E) hysteresis loop (b) and energy storage properties (c) of the composites.

high frequency.[27] As shown in Fig. 2(a1), the permittivity of the film increases from the value of ~11 for the sandwich-structured composite with central terpolymer PTC to the value of ~16 for the composites with introduced central terpolymer PTCF layers due to the much larger aspect ratio of the P(VDF-TrFE-CFE) fiber. Here, when the thickness ratio of three layers for the sandwich-structured composite is about 9:16:9, the overall dielectric permittivity of the P/PTCF/P film (ε_r) can be given by the dielectric permittivity of the outer PVDF layer ($\varepsilon_p \sim 10.2$, referring to Fig. S3 of the supplementary material) and the central P(VDF-TrFE-CFE) fiber layer ($\varepsilon_c \sim 56$) as

$$\varepsilon_r = \frac{17\varepsilon_p\varepsilon_c}{8\varepsilon_p + 9\varepsilon_c}. \tag{2}$$

As the calculated result, the serial equivalent model of ε_r for the P/PTCF/P composite is about 16.6, which is well consistent with the experimental result (~16). It is interesting that the orientation polarization of the central PTCF fiber layer with large aspect ratio in this work. Simultaneously, the non-polar γ phase is preferred to be formed, inducing by the quenching process in the PVDF and the P(VDF-TrFE-CFE), which contributes to improving the dielectric permittivity. Apparently, the dielectric permittivity of films with the quenching process is higher than that of films without the quenching process. Figure 2(a2) shows the variations in the conductivity and dielectric loss as functions of frequency for composites. The conductivity of sandwich-structured composites with a central terpolymer PTC and PTCF layer possesses a high dependence on frequency and a low value, indicating an insulating characteristic. The electronic transmission was controlled to get a lower conductivity, so the dielectric loss reduced at low frequency ($<10^4$ Hz). With the central terpolymer layer introduced, the conductivity of the composite has a small increasing fluctuation, and also it holds in a lower magnitude due to the good compatibility. As presented in Fig. 2(a2), with the frequency increasing, the faster the electric field switches, the more the dipole relaxation[28,29] gradually happens, and the higher dielectric loss of the film is. Obviously, there are relaxation peaks in Fig. 2(a2) at the frequency of ~4 MHz, which evidenced the existence of the polar β phase without quenching composites.[29–31]

Figure 2(b) presents the *D-E* loops, the discharged energy density (U_e), and the discharged efficiency (η) of sandwich-structured composites at 10 Hz; meanwhile, the values of U_e are calculated from the *D-E* loops [Fig. 2(b)] and η is calculated by η = *Discharge energy*/*Charge energy*, and then they are plotted in Fig. 2(c). The most seductive feature in Fig. 2(b) is the notable increase of maximal displacement (D_m) because of the quenching process and the central terpolymer PTCF layer. Such as the D_m of the composite with the PTCF central layer increases from ~4.76 μC/cm^2 without a quenching film to ~6.09 μC/cm^2 with a quenching film at 300 kV/mm because of the formation of γ phase with the quenching process which is more likely that the ferroelectric is replaced by paraelectric.[25,32] Owing to the enhanced electric polarization and absence of early polarization saturation,[25] the quenched films exhibit consistently higher U_e at every applied electric field comparing with films without quenching. As can be seen from Fig. 2(c2), the introduced central terpolymer PTCF layer can markedly improve U_e of the composite, such as U_e increases from ~3.3 J/cm^3 for the P/PTC/P composite with quenching at 220 kV/mm to ~8.7 J/cm^3 for the P/PTCF/P composite with quenching at 360 kV/mm, mainly because of the improved electric field strength and the enhanced electric displacement of the composite.[23]

Meanwhile, the discharged efficiency maintains at a high value, for instance, η increases from ~52% for the P/PTC/P composite with quenching to ~69% for the P/PTCF/P composite with quenching at the same electric field of 220 kV/mm; this may be attributed to the suppressed D_r by an obvious non-polar γ phase[23,25] and the enhanced electric displacement by the introduced P(VDF-TrFE-CFE) fibers.[23] Furthermore, η of the composite with a PTCF central layer reaches ~60% at the electric field strength of 360 kV/mm, which could be contributed to the low leakage current of the PTCF central layer in the composite.[5]

Figure 3(a) is the leakage current of the sandwich composite with the central layer of PTC and PTCF. As shown in Fig. 3(a), the leakage current of all composites maintains at the lower order of 10^{-6} A/cm^2. It is worth noting that the leakage current of the composite with the central PTCF keeps in a lower order of magnitude (10^{-7} A/cm^2) before the electric field of 250 kV/mm. This can be understood that the central fiber layer of the sandwich structure acts a role of barrier against the

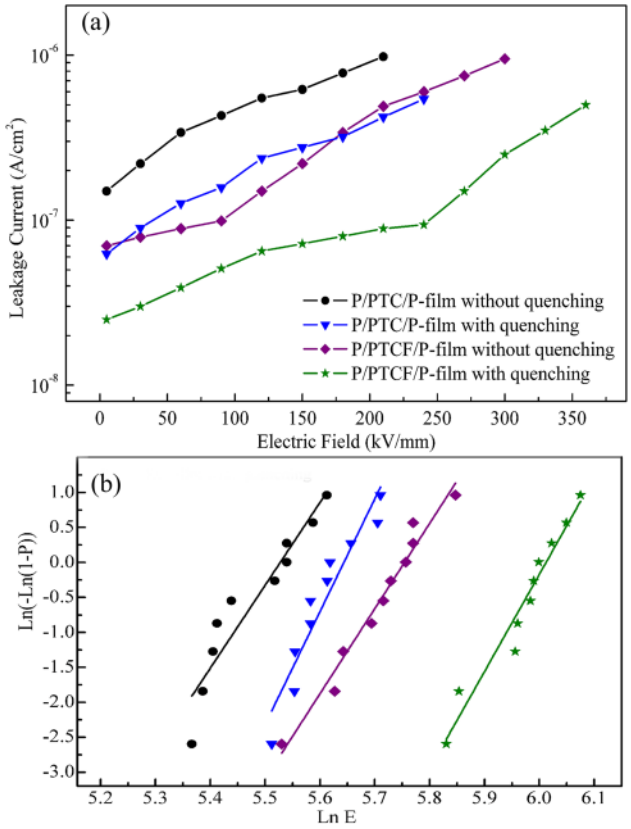

FIG. 3. The leakage current *vs.* electric field (a) and the Weibull distribution of breakdown strength (b) for the sandwich-structured composites.

electronic and the space-charge conduction. In addition to the phase transformation, the crystalline structures were changed from the high hysteresis loss of the ferroelectric β phase to low loss of the paraelectric γ phase after the quenching process.[14,15,23,33,34]

Additionally, the breakdown strength is another key for dielectric materials, so it was tested at room temperature under the DC electric field. And the values were described by the Weibull cumulative distribution function with two parameters as $P(E) = 1 - \exp(-(E/E_b)^{\beta})$, where $P(E)$ represents the cumulative probability of failure, E means the experimental breakdown strength, E_b is the scale parameter referring to the breakdown strength at the cumulative failure probability of 63.2%, and β represents the shape parameter describing the linear regressive fit of the distribution.

This formula also can be written as follows: $\ln(-\ln(1 - P(E))) = \beta \ln E - \beta \ln E_b$, then $\ln(-\ln(1 - P(E)))$ versus $\ln E$ was plotted in Fig. 3(b). The liner fitting results and Weibull parameters are shown in Table SI of the supplementary material. Apparently, the breakdown strength of the composite with the PTCF central layer (408 kV/mm) is greater than any others because the growth of the inner electrical treeing may be hindered by the P(VDF-TrFE-CFE) fibers between outer layers.[8,35]

To prove the above results, it is crucial to investigate the distribution of local electric fields among the layers of the sandwich-structured composite.[5,36] When there is a dielectric difference, the redistribution of local electric fields will happen. And the local electric fields of series layers can be given by

$$E_p = \frac{E_b\left(2d_p + d_c\right)}{2d_p + \frac{\varepsilon_p}{\varepsilon_c}d_c}, \tag{3}$$

$$E_c = \frac{E_b\left(2d_p + d_c\right)}{d_c + 2\frac{\varepsilon_c}{\varepsilon_p}d_p}, \tag{4}$$

where E_p and E_c are the local electric fields of the outer P layer and central PTCF layer, respectively. E_b means the breakdown strength, d_p and d_c represent the thickness of the outer P layer and central PTCF layer, respectively. If ε_p of the outer P layer is ~10.2 (referring to the Fig. S3 of the supplementary material) and ε_c of the central PTCF layer is ~56, d_p of the outer layer is about 9 μm and d_c of the central layer is about 16 μm, and E_b is ~408 kV/mm, as a result, E_p of ~663 kV/mm and E_c of ~120 kV/mm can be gained by the above voltage division formulas of the series capacitor. The local electric field of the outer P layer is about 5.5 times larger than that of the central PTCF layer. The redistribution of the electric field can be advantageous to improve the electric displacement of the outer layer and to reduce the probability of breakdown for the central layer to enhance the overall E_b of the composite. Additionally, a lower local electric field of the central layer can hinder the expansion of electrical treeing.[5,6] Moreover, the large aspect ratio of the P(VDF-TrFE-CFE) fibers, which may weaken the growth of the electrical treeing, contributes to enhancing the breakdown strength of the sandwich-structured composite. Meanwhile, the non-polar γ phase may reduce the failure probability of the breakdown strength. Here, we give the principle model of the mechanism on the redistribution of internal electric fields and the inhibition of electrical treeing in Fig. S4 of the supplementary material, which indicates that the growth of the electrical treeing is gradually weakened due to the scattering by the central fibers.

In summary, the P(VDF-TrFE-CFE) fiber was fabricated by the electrospinning process, and the single films were prepared by a solution-casting method, then the P(VDF-TrFE-CFE) fiber layer was introduced and compound with the PVDF film to obtain the sandwich-structured composite with excellent dielectric permittivity as well as energy density. The reason was that the lower local electric field of the central layer of the P(VDF-TrFE-CFE) fiber inhibited the electrical treeing process under an applied voltage. And the P(VDF-TrFE-CFE) fiber layer showed a good compatibility with the PVDF layer, which was beneficial for enhancing the dielectric property and the breakdown strength of the film. The permittivity of the sandwich-structured composite reached ~16, the maximum discharged energy density ran up to ~8.7 J/cm^3 at 360 kV/mm, and the breakdown strength was up to about 408 kV/mm, all of which were obvious advantages in practical application for the electronics industry.

See supplementary material for experimental methods, supplemental results, and additional figures.

The authors gratefully thank the support of the National Natural Science Foundation of China (No. 61640019), the Open Foundation of State Key Laboratory of Electronic Thin Films and Integrated Devices (No. KFJJ201601), Science Funds for the Young Innovative Talents of HUST (No. 201102).

[1] B. Chu, X. Zhou, K. Ren, B. Neese, M. Lin, Q. Wang, F. Bauer, and Q. M. Zhang, Science **313**, 334 (2006).
[2] C. H. Zhang, Q. G. Chi, J. F. Dong, Y. Cui, X. Wang, L. Z. Liu, and Q. Q. Lei, Sci. Rep. **6**, 33508 (2016).
[3] P. Kim, N. M. Doss, J. P. Tillotson, P. J. Hotchkiss, M. J. Pan, S. R. Marder, J. Li, J. P. Calame, and J. W. Perry, ACS Nano **3**, 2581 (2009).
[4] V. Sharma, C. Wang, R. G. Lorenzini, R. Ma, Q. Zhu, D. W. Sinkovits, G. Pilania, A. R. Oganov, S. Kumar, and G. A. Sotzing, Nat. Commun. **5**, 4845 (2014).
[5] Y. Shen, D. S. Shen, X. Zhang, J. Y. Jiang, Z. K. Dan, Y. Song, Y. H. Lin, M. Li, and C. W. Nan, J. Mater. Chem. A **4**, 8359 (2016).
[6] X. Zhang, Y. Shen, B. Xu, Q. H. Zhang, L. Gu, J. Y. Jiang, J. Ma, Y. H. Lin, and C. W. Nan, Adv. Mater. **28**, 2055 (2016).
[7] Q. G. Chi, J. Sun, C. H. Zhang, G. Liu, J. Q. Lin, Y. N. Wang, X. Wang, and Q. Q. Lei, J. Mater. Chem. C **2**, 172 (2014).
[8] Y. Song, Y. Shen, H. Y. Liu, Y. H. Lin, M. Li, and C. W. Nan, J. Mater. Chem. **22**, 8063 (2012).
[9] Q. G. Chi, J. F. Dong, C. H. Zhang, C. P. Wong, X. Wang, and Q. Q. Lei, J. Mater. Chem. C **4**, 8179 (2016).
[10] Z. Zhou, C. C. Bowland, M. H. Malakooti, H. Tang, and H. A. Sodano, Nanoscale **8**, 5098 (2016).
[11] Q. G. Chi, T. Ma, J. F. Dong, Y. Cui, Y. Zhang, C. H. Zhang, S. C. Xu, X. Wang, and Q. Q. Lei, Sci. Rep. **7**, 3072 (2017).
[12] S. J. Laihonen, U. Gafvert, T. Schutte, and U. W. Gedde, IEEE Trans. Dielectr. Electr. Insul. **14**, 275 (2007).
[13] B. Xie, Q. Zhang, H. B. Zhang, G. Z. Zhang, S. Y. Qiu, and S. L. Jiang, Ceram. Int. **42**, 19012 (2016).
[14] D. Guo, K. Cai, and Y. L. Wang, J. Mater. Chem. C **5**, 2531 (2017).
[15] Prateek, V. K. Thakur, and R. K. Gupta, Chem. Rev. **116**, 4260 (2016).
[16] L. Yao, D. R. Wang, P. H. Hu, B. Z. Han, and Z. M. Dang, Adv. Mater. Interfaces **3**, 1600016 (2016).
[17] M. S. Zheng, J. W. Zha, Y. Yang, P. Han, C. H. Hu, and Z. M. Dang, Appl. Phys. Lett. **109**, 072902 (2016).
[18] Y. Li, Q. Fu, L. L. Li, and W. P. Li, J. Electron. Mater. **45**, 5152 (2016).
[19] Y. Chen, B. Lin, X. Zhang, J. Wang, C. Lai, Y. Sun, Y. Liu, and H. Yang, J. Mater. Chem. A **2**, 14118 (2014).
[20] Y. Wang, J. Cui, Q. Yuan, Y. Niu, Y. Bai, and H. Wang, Adv. Mater. **27**, 6658 (2015).
[21] J. W. Zha, Z. M. Dang, T. Yang, T. Zhou, H. T. Song, and S. T. Li, IEEE Trans. Dielectr. Electr. Insul. **19**, 1312 (2012).
[22] P. H. Hu, J. Wang, Y. Shen, Y. H. Guan, Y. Lin, and C. W. Nan, J. Mater. Chem. A **1**, 12321 (2013).
[23] X. Zhang, Y. Shen, Z. H. Shen, J. Y. Jiang, L. Q. Chen, and C. W. Nan, ACS Appl. Mater. Interfaces **8**, 27236 (2016).

[24] W. J. Li, Q. J. Meng, Y. S. Zheng, Z. C. Zhang, W. M. Xia, and Z. Xu, Appl. Phys. Lett. **96**, 192905 (2010).
[25] H. Tang and H. A. Sodano, Nano Lett. **13**, 1373 (2013).
[26] P. Khanchaitit, K. Han, M. R. Gadinski, Q. Li, and Q. Wang, Nat. Commun. **4**, 2845 (2013).
[27] X. D. Zhao, J. P. Cao, J. Zhao, G. H. Hu, and Z. M. Dang, J. Mater. Chem. A **2**, 10614 (2014).
[28] Y. Xie, Y. Yu, Y. Feng, W. Jiang, and Z. Zhang, ACS Appl. Mater. Interfaces **9**, 2995 (2017).
[29] F. H. Wang, Y. Kong, Z. Liu, and H. Zhu, Polym. Plast. Technol. Eng. **56**, 526 (2017).
[30] Y. F. Wang, J. Cui, L. X. Wang, Q. B. Yuan, Y. J. Niu, J. Chen, Q. Wang, and H. Wang, J. Mater. Chem. A **5**, 4710 (2017).
[31] C. H. Zhang, Q. G. Chi, L. Z. Liu, Y. Chen, J. F. Dong, T. Ma, X. Wang, and Q. Q. Lei, J. Mater. Sci.: Mater. Electron. **28**, 2502 (2017).
[32] J. J. Wang, X. Q. Ma, Q. Li, J. Britson, and L. Q. Chen, Acta Mater. **61**, 7591 (2013).
[33] Q. Li, G. Z. Zhang, F. H. Liu, K. Han, M. R. Gadinski, C. X. Xiong, and Q. Wang, Energy Environ. Sci. **8**, 922 (2015).
[34] Y. F. Hou, Y. Deng, Y. Wang, and H. L. Gao, RSC Adv. **5**, 72090 (2015).
[35] G. Y. Wang, X. Y. Huang, and P. K. Jiang, ACS Appl. Mater. Interfaces **7**, 18017 (2015).
[36] P. H. Hu, Y. Shen, Y. H. Guan, X. H Zhang, Y. H. Lin, Q. M. Zhang, and C. W. Nan, Adv. Funct. Mater. **24**, 3172 (2014).